Molecules and Cells

Dynamic Changes in the Bridging Collaterals of the Basal Ganglia Circuitry Control Stress-Related Behaviors in Mice

Young Lee[1], Na-Eun Han[1], Wonju Kim[1], Jae Gon Kim[1], In Bum Lee[1], Su Jeong Choi[7], Heejung Chun[2], Misun Seo[3,4], C. Justin Lee[2], Hae-Young Koh[3,4], Joung-Hun Kim[5], Ja-Hyun Baik[1], Mark F. Bear[6], Se-Young Choi[7], and Bong-June Yoon[1,*]

[1]Department of Life Sciences, Korea University, Seoul 02841, Korea, [2]Cognitive Glioscience Group, Center for Cognition and Sociality, Institute for Basic Science (IBS), Daejeon 34126, Korea, [3]Center for Neuroscience, Brain Science Institute, Korea Institute of Science and Technology (KIST), Seoul 02792, Korea, [4]Department of Neuroscience, University of Science and Technology (UST), Daejeon 34113, Korea, [5]Department of Life Sciences, Pohang University of Science and Technology (POSTECH), Pohang 37673, Korea, [6]The Picower Institute for Learning and Memory, Department of Brain and Cognitive Sciences, Massachusetts Institute of Technology, Cambridge, MA 02139, USA, [7]Department of Physiology and Neuroscience, Dental Research Institute, Seoul National University School of Dentistry, Seoul 03080, Korea
*Correspondence: bjyoon69@korea.ac.kr
https://doi.org/10.14348/molcells.2019.0279
www.molcells.org

The basal ganglia network has been implicated in the control of adaptive behavior, possibly by integrating motor learning and motivational processes. Both positive and negative reinforcement appear to shape our behavioral adaptation by modulating the function of the basal ganglia. Here, we examined a transgenic mouse line (G2CT) in which synaptic transmissions onto the medium spiny neurons (MSNs) of the basal ganglia are depressed. We found that the level of collaterals from direct pathway MSNs in the external segment of the globus pallidus (GPe) ('bridging collaterals') was decreased in these mice, and this was accompanied by behavioral inhibition under stress. Furthermore, additional manipulations that could further decrease or restore the level of the bridging collaterals resulted in an increase in behavioral inhibition or active behavior in the G2CT mice, respectively. Collectively, our data indicate that the striatum of the basal ganglia network integrates negative emotions and controls appropriate coping responses in which the bridging collateral connections in the GPe play a critical regulatory role.

Keywords: basal ganglia, bridging collaterals, globus pallidus, stress

INTRODUCTION

The basal ganglia network consists of multiple subcortical nuclei interconnected: the striatum, the globus pallidus (GP), the subthalamic nucleus, and the substantia nigra (SN). Impairments in cellular functions or neural activity in the basal ganglia are closely associated with profound deficits in motor regulations, as observed in several movement disorders (DeLong, 1990). It has long been postulated that the basal ganglia controls the initiation of movement by selecting an appropriate action while inhibiting competing actions (Mink, 1996). The striatum is the major input structure in the basal ganglia, integrating cortical, thalamic, and mesolimbic innervations. There are two parallel projections from distinct subpopulations of striatal medium spiny neurons (MSNs),

Received 19 November, 2019; revised 13 December, 2019; accepted 17 December, 2019; published online 14 January, 2020

eISSN: 0219-1032

the major cell type in the striatum. Dopamine receptor type 1 (D1)-expressing MSNs (D1-MSNs) primarily project their axons to the substantia nigra pars reticulata (SNr) to form the direct pathway while dopamine receptor type 2 (D2)-expressing MSNs (D2-MSNs) project to the external segment of the GP (GPe) to form the indirect pathway (Gerfen et al., 1990).

According to the classical model of basal ganglia circuit function, the direct pathway promotes specific motor programs, whereas the indirect pathway suppresses competing motor programs (Albin et al., 1989; DeLong, 1990; Roseberry et al., 2016). In support of the classical model, studies in which the neuronal integrity or activity were manipulated in a pathway-specific manner demonstrated that the two parallel pathways play distinct and contrasting roles in physiological and behavioral functions (Bateup et al., 2010; Hikida et al., 2010; Kim et al., 2017a; Kravitz et al., 2010; 2012; Kreitzer and Malenka, 2007; Shen et al., 2008). However, other studies selectively measured the endogenous activity of these pathways in naturalistic movements and found that the neural activity of both pathways is concurrently increased, particularly during action initiation (Cui et al., 2013; Jin et al., 2014; Tecuapetla et al., 2014; 2016). These studies have suggested that fine coordination of the two pathways is required for uninterrupted action initiation and execution. Precise and dynamic coordination of activity patterns and timing is highly likely to depend on complex interconnections between the two pathways. In addition to direct collateral connections from D2-MSNs to D1-MSNs within the striatum (Taverna et al., 2008; Tecuapetla et al., 2009), collateral connections made by D1-MSNs in the GPe ("bridging collaterals") may also be an important means to coordinate the activity of the two pathways (Cazorla et al., 2014; Fujiyama et al., 2011; Kawaguchi et al., 1990; Wu et al., 2000).

Here, we explore the functional role of the basal ganglia circuits under the conditions of predator-induced stress. In the presence of detected threats, animals must select a defensive tactic that should increase the probability of organismal survival (LeDoux, 2012). We questioned whether the basal ganglia network affects behavior under stress. Our study revealed that altered synaptic transmissions in the striatum, the major input structure of the basal ganglia, modified the behavior of transgenic mice after being exposed to predator stress (PRST). Furthermore, we found that dynamic changes in the density of collateral connections from D1-MSNs to the GPe significantly affected the behavioral output. Our data suggest that the bridging collaterals may control the output activity of the basal ganglia network by adjusting the balance between the two pathways. These findings may have important implications in elucidating the pathophysiology of certain psychiatric disorders such as anxiety disorders.

MATERIALS AND METHODS

Animals

We used adult male mice (10-14 weeks old at the time of behavioral analyses) in all the experiments except for those involving designer receptors exclusively activated by designer drugs (DREADDs). We used both males and females in the DREADD experiments because we did not find significant gender differences in the experiments.

Drd1a-CRE (EY217Gsat/Mmcd, termed D1-CRE in our study) and Drd2-CRE (ER44Gsat/Mmcd, termed D2-CRE in our study) mice were purchased from Mutant Mouse Regional Resource Centers (MMRRC) at UC Davis (USA). D1-CRE mice were crossed with G2CT mice to obtain D1-CRE:CaMKIIα-tTA:G2CT triple transgenic mice for the bridging collaterals study. For predator odor presentation, male Crl:CD (SD) rats were purchased from Orient Bio (Korea).

Animals were maintained in the Gyerim Experimental Animal Resource Center of Korea University under standard conditions at 23 ± 1°C with 12-h light-dark cycles (7 AM/7 PM) and with food and water available *ad libitum*.

All experimental procedures using animals were approved by the Institutional Animal Care and Use Committee of Korea University (KUIACUC-2019-0039).

Generation of G2CT mice

For the G2CT-expressing transgenic mice, we built a transgene construct in which the peptide sequence is under the control of the Tet-responsive element. We amplified a 93-bp cDNA encoding section of the GluR2 carboxy-terminal cytoplasmic tail by reverse transcription polymerase chain reaction (RT-PCR) using primers spanning the region (G2ct-Xho5'; 5'-cctcgagatgctggtggctttgattgag-3', G2ct-Age3'; 5'-accggtctaagatgggttaatattctgtgc-3') and cloned it into the pBI-EGFP Tet vector. Then, it was mutagenized to generate a deletion that disrupts N-ethylmaleimide sensitive fusion protein (NSF) binding (KRMKLNINP) using the QuickChange site-directed mutagenesis system (Stratagene, USA). This modified polypeptide, termed G2CT, contains an intact AP2 binding sequence but not an NSF binding sequence. The final construct was digested with Aat II and Ase I to isolate the 3.2-kb transgene used for pronuclei injection. Positive candidate founder lines were crossed with the B40 transgenic line that expresses tTA under the CaMKIIα promoter to obtain double transgenic mice in which the expression of the transgene can be restricted with spatial and temporal specificity. The double transgenic mice (termed G2CT mice for simplicity) were used in our study, and littermates carrying a single transgene (G2CT or tTA) or no transgene were used as controls.

Drug

Haloperidol hydrochloride (#0931; Tocris, UK) dissolved in 2% DMSO/0.9% NaCl solution was administered subcutaneously in the interscapular region for 14 days (0.5 mg/kg; three times a day).

Clozapine N-oxide (CNO) (#4936; Tocris) dissolved in saline was injected intraperitoneally 30 min prior to the behavioral tests (10 mg/kg) or administered intraperitoneally every 12 h for 14 days (1 mg/kg).

Virus preparation

pAAV-ef1α-DIO-EYFP (pAAV-DIO-EYFP) was generously provided by Dr. Karl Deisseroth. pAAV-hSyn-DIO-hM3D(Gq)-mCherry (pAAV-DIO-hM3Dq) was a gift from Dr. Bryan Roth (Addgene plasmid #44361). pAAV-CAG-FLEX-tdTomato (pAAV-FLEX-tdTomato) was a gift from Dr. Edward Boyden (Addgene plasmid #28306).

The AAV-DIO-EYFP, AAV-EYFP, AAV-DIO-hM3Dq, AAV-hM3Dq, AAV-FLEX-tdTomato and AAV-tdTomato were prepared with the use of the AAV Helper-Free System (Cat#240071; Agilent Technologies, USA) following the manufacturer's protocol. The viral titer was measured in HT-1080 cells via flow cytometry (Lambeth et al., 2005). The titer of the viruses was as follows (in infectious unit [IU]/μl): AAV-DIO-hM3Dq, 9.1×10^8; AAV-DIO-EYFP, 4.4×10^8; AAV-hM-3Dq, 6.1×10^8; AAV-tdTomato, 5.8×10^8; AAV-FLEX-tdTomato, 3.2×10^8.

Stereotaxic injections

Stereotaxic injections were performed on 8- to 9-week-old mice. The animals were anaesthetized with a mixture of ketamine (100 mg/kg) and xylazine (10 mg/kg) via intraperitoneal injection and secured in a stereotaxic apparatus. For stereotaxic injection, glass micropipettes and the Nanoliter 2000 (World Precision Instrument, USA) were used to inject the virus. The following stereotaxic coordinates were used (in mm; relative to bregma): for behavioral studies, AAV-DIO-hM3Dq, AAV-DIO-EYFP, AAV-hM3Dq, and AAV-tdTomato were bilaterally injected (AP +1.1, ML ±1.1, DV −3.25); for measurement of the bridging collateral with haloperidol injection, AAV-FLEX-tdTomato was injected at two sites (site A: AP +1.3, ML ±1.4, DV −3.2; site B: AP +0.8, ML ±2.0, DV −3.4); for the measurements of the bridging collateral with CNO injection, a viral mixture of AAV-DIO-EYFP and AAV-hM3D (1:1(v/v)) was bilaterally injected (AP +1.1, ML ±1.1, DV −3.25). The injection rate for all AAV vectors was 23.0 nl/sec/injection (10 injections total with a 20-s interval). The glass pipette was left in place for 10 min after the final injection and then slowly withdrawn.

Behavioral tests

All behavioral tests except the acoustic startle response test were conducted in a soundproof behavioral chamber under bright illumination (100 lux). Mice behavior in the tests was video-recorded and the movies were analyzed with the video tracking software EthoVision XT 11.5 (Noldus, USA).

PRST exposure

For PRST exposure, a cage containing the subject mice was placed in a large translucent plastic container (52 cm × 68 cm × 44 cm) with a cage containing a rat (450-600 g). An opaque divider between the mouse and rat cages prevented visual contact. The container was covered with a lid to enhance the olfactory stimulation. The PRST exposure lasted overnight (16-18 h).

Elevated plus maze (EPM) test

The EPM consisted of two open arms (67 cm × 7 cm × 0.5 cm) and two closed arms (67 cm × 7 cm × 17 cm). The closed arms were enclosed in a 17-cm wall, and the apparatus was raised 57 cm above the ground. After 1-h habituation in the behavioral chamber, the mouse was placed in the center of the maze facing an open arm and allowed to freely explore the maze for 5 min. For movement analysis, we used the same parameters as previously described (Kravitz et al., 2010). Briefly, ambulation was defined as periods when the speed of the animal (center point) averaged more than 2 cm/s for at least 0.5 s. Freezing was defined as periods when the pixel changes in the mouse image averaged less than 2% for at least 1 s. Fine movement was defined as any movement that was not ambulation or freezing. To analyze the risk-assessing behavior, the number of head dips (downward movement of rodents' head toward the floor from the open arms) was manually counted.

Open field test (OFT)

An open field apparatus was assembled with white acrylic containers (30 cm × 30 cm × 40 cm). After a 20-min habituation in the chamber, animals were placed in the center of the apparatus. The open field was divided into a central zone (12 cm × 12 cm) and a peripheral zone. Animals were allowed to freely explore the apparatus for 60 min.

Acoustic startle response

Mice were placed in a cylinder and acclimated to the startle chamber (San Diego Instruments, USA) for 5 min. Background white noise (65 dB) was present during this adaptation period and throughout the session. The session started with four 40-ms 120-dB bursts of white noise. The behavior of the mice during these bursts was not included in the analysis because the responses to the first few startle bursts generally differ in magnitude from the rest of the trials. Six different intensities of acoustic stimuli were used (70, 80, 90, 100, 110, and 120 dB). The duration of the stimuli was 40 ms and they were randomly presented 10 times. The time between the stimuli averaged 15 s but this interval was varied within a range of 5-30 s so that the animals did not anticipate the stimulus.

Accelerating rotarod

Motor coordination and balance were assessed on an accelerating rotarod (EVN-577M; MED Associates, USA) as described previously with minor modifications (Stroobants et al., 2013). After a training session (4 rpm, 2 min; with constant speed), accelerating rotarod tests (three 5 min trial with 10 min intertrial interval) were performed. During the test trial, mice were placed on a rotating rod that accelerated from 4 to 40 rpm in 5 min, beginning 10 s after the mouse was placed on the rod. The trial duration was counted from the start of the acceleration. The latency to fall off of the rotarod was recorded, and the mean latency to fall for the three trials was analyzed.

Marble burying test (MBT)

Marble burying behavior was evaluated as previously described with minor modifications (Deacon, 2006). We used an open field apparatus (30 cm × 30 cm × 40 cm) as the test box to perform the MBT. The test box was filled with woodchip bedding that was approximately 5 cm deep, and lightly tamped down to make a flat and even surface. Then, 25 glass marbles (approximately 15 mm diameter) were placed on the surface, evenly spaced at approximately 4 cm apart, and lightly tamped down to fix them in position. After a 20-min habituation in the soundproof chamber, the animal was placed in the test box and left for 30 min, then the number of marbles buried (to 2/3 their depth) in the bedding were

counted.

Immunohistochemistry

Mice were deeply anaesthetized with a mixture of ketamine (150 mg/kg) and xylazine (15 mg/kg) and their brains were fixed through cardiac perfusion with chilled 4% paraformaldehyde (PFA) in phosphate-buffered saline (PBS). The striatum was serially sectioned into 40-μm-thick slices on a cryostat (Leica CM1950; Leica, Germany). The free-floating sections were incubated with blocking buffer (3% bovine serum albumin, 0.5% Triton X-100 in 0.1 M PBS) for 1 h, and incubated with a primary antibody in blocking buffer overnight at 4˚C. The sections were subsequently incubated with a secondary antibody in blocking buffer for an hour at RT. The sections were rinsed with PBST and mounted with mounting medium.

The primary antibodies used in immunostaining were as follows: c-fos (1:80, SC-52-G; Santa Cruz Biotechnology, USA); mCherry (1:1,000, ab167453; Abcam, UK); DARPP-32 (1:200, #2302; Cell Signaling Technology, USA), choline acetyltransferase (ChAT) (1:1,200, AB144P; Millipore, USA), Substance P (SP) (1:100, SC-58591; Santa Cruz Biotechnology), or D2R (1:100, AB5084P; Millipore); Synaptophysin (SYP) (1:100, SC-17750; Santa Cruz Biotechnology); GFP (1:1,000, GFP-1020; Aves Labs, USA); FOXP2 (1:100, ab1307; Abcam); and Parvalbumin antiserum (PV) (1:500, PVG-213; Swant, Switzerland).

The secondary antibodies used in immunostaining were as follows: anti-goat IgG Alexa Fluor 488 (1:400, A-11055; Thermo Fisher Scientific, USA); anti-rabbit IgG Alexa Fluor 594 (1:400, A-21207; Thermo Fisher Scientific); anti-rabbit IgG Alexa Flour 568 (1:400, A-11011; Thermo Fisher Scientific); anti-goat IgG Alexa Flour 568 (1:400, A-11057; Thermo Fisher Scientific); anti-mouse IgG Alexa Fluor 594 (1:200, A-21203; Thermo Fisher Scientific); anti-mouse IgG Alexa Flour 405 (1:200, A-31553; Thermo Fisher Scientific); donkey anti-goat IgG Alexa Flour 405 (1:400, ab175664; Abcam); and anti-chicken IgY Alexa Flour 488 (1:400, 705-545-155; Jackson ImmunoResearch Laboratories, USA).

Slice preparation and surface receptor biotinylation

The α-amino-3-hydroxy-5-methylisoxazole-4-propionic acid receptor (AMPAR) surface expression was measured using biotinylation as described previously with minor modifications (Yoon et al., 2009). Striatal slices (300-μm-thick) were prepared using a vibratome (Campden Instruments, England) and allowed to recover in carbogenated (5% CO_2 and 95% O_2) artificial cerebrospinal fluid (ACSF) supplemented with 1 μM Latrunculin A (#3973; Tocris) at 30˚C for 2 h. After recovery, the slices were transferred to ice-cold sulfo-NHS-LC-biotin (Thermo Fisher Scientific) in ACSF (1 mg/ml) and incubated for 20 min on ice. Then, they were washed three times (1× with ice-cold TBS, 2× with ice-cold ACSF) and microdissected to separate the dorsal striatum from the slices. The pieces of the dorsal striatum were homogenized in RIPA buffer supplemented with 0.5% (v/v) protease inhibitor cocktail (#535140; Calbiochem, USA). Homogenates were incubated on ice for 15 min, then centrifuged (14,000*g*) for 15 min at 4˚C. The supernatant was collected, and the protein concentration was measured. Extracts containing 60 μg of protein were mixed with 60 μl Neutravidin (Thermo Fisher Scientific) and incubated overnight at 4˚C. The following day, the biotinylated protein–avidin complex was washed (3× with RIPA buffer), then resuspended in SDS sample buffer (45 μl), and boiled for 10 min. The total protein (avidin-unbound) and pulled-down protein (avidin-bound) samples were used for an immunoblotting assay (GluA1, AB1504; GluA2, MAB397; neural cell adhesion molecule [NCAM], AB5032; Actin, MAB1501; all antibodies were purchased from Millipore). The surface levels of AMPARs were normalized to the level of NCAM.

Corticosterone (CORT) analysis

Blood samples for CORT measurement were collected prior to PRST exposure (basal) and immediately after the end of PRST exposure. All samples were collected between 4:00 PM and 5:00 PM. After the mice were removed from their home cages, 20-30 μl of blood was rapidly collected from the lateral tail vein using heparinized capillary tubes (Kimble Chase, USA). The blood samples were centrifuged for 10 min at 14,000*g* at 4˚C, then the supernatant (plasma) was collected and stored at −80˚C until analysis. The plasma CORT level was measured using a CORT enzyme-linked immunosorbent assay kit (Assay Design, USA) according to the manufacturer's recommended protocol.

Structural analysis of dendritic spines

Tissue sampling for dendritic spine analysis was conducted as previously described (Kim et al., 2013). Briefly, coronal slices (200 μm thick) containing the striatum were prepared using a vibratome. Brain slices were fixed with 4% PFA in PBS on ice for 30 min and subjected to biolistic labeling using a gene gun (Bio-Rad, USA) at 100 psi helium pressure with DiI-coated tungsten particles (Molecular Probes, USA). The slices were washed in PBS and mounted on slides using mounting medium (VECTASHIELD). All DiI-labeled cells with a clear soma and spiny dendrites were selected for imaging. For the G2CT-expressing cells, cells that expressed GFP were selected. Confocal images of the cells were acquired using a Carl Zeiss LSM 700 confocal fluorescence microscope (Zeiss, Germany) equipped with a Plan-Apochromat 63×/1.40 oil-immersion objective and 0.343-μm z-step size. Dendritic spine analysis was performed using NeuronStudio (http://research.mssm.edu/chic/tools-ns.html) as described previously (Rodriguez et al., 2008). All spine-like protrusions and dendritic length were measured in dendritic segments (region between two neighboring branch points), and the total measurements were divided by the length of the dendritic segment to obtain the average number per unit length (10 μm). Protrusions under 3.0 μm and over 0.2 μm in length were considered spine-like. The criteria used for morphological classification of the spines were as follows: thin spines, spine length (L) / head diameter (dh) ≥ 2.5 (except for the spines that met the criteria for mushroom spines); mushroom spines, dh / neck diameter (dn) > 1.1, dh ≥ 0.35 μm; stubby spines, L / dh < 2.5, dh < 0.35 μm. All image analyses were performed in a blinded fashion.

Electrophysiological recording

Slice preparation

Animals were anesthetized with isoflurane and immediately decapitated. The brains were rapidly removed and submerged in ice-cold, oxygenated (95% O_2 and 5% CO_2), low-Ca^{2+}/high-Mg^{2+} dissection buffer containing 5 mM KCl, 1.23 mM NaH_2PO_4, 26 mM $NaHCO_3$, 10 mM dextrose, 0.5 mM $CaCl_2$, 10 mM $MgCl_2$, and 212.7 mM sucrose. Coronal slices of the dorsomedial striatum (DMS) were cut at a thickness of 300 μm (for whole-cell patch clamp recordings) with a vibratome (5100 mz; Campden Instruments). Slices containing the DMS were placed in a holding chamber in an incubator containing oxygenated (95% O_2 and 5% CO_2) ACSF with 124 mM NaCl, 5 mM KCl, 1.23 mM NaH2PO_4, 2.5 mM $CaCl_2$, 1.5 mM $MgCl_2$, 26 mM $NaHCO_3$, and 10 mM dextrose at 28-30°C for at least 30 min.

Whole-cell patch clamp recordings

Whole-cell, patch-clamp recordings from MSNs in the DMS slices were performed as described previously with minor modifications (Choi et al., 2018). Briefly, slices were transferred to a recording chamber where they were continuously perfused with oxygenated ACSF (95% O_2 and 5% CO_2) at a flow rate of 2 ml/min at 25°C. Whole-cell voltage clamp recordings were obtained using a Multiclamp 700A amplifier (Molecular Devices, USA), and slices were visualized using infrared differential interference contrast video microscopy (BX51WI; Olympus, Japan). Signals were filtered at 2 kHz and digitized at 10 kHz using Digidata 1440 (Molecular Devices).

The patch pipette electrodes (4-6 MΩ) used to record AMPAR-mediated excitatory postsynaptic currents (EPSCs) contained 130 mM $CsMeSO_4$, 0.5 mM EGTA, 5 mM TEA-Cl, 8 mM NaCl, 10 mM HEPES, 1 mM QX-314, 4 mM Mg-ATP, 0.4 mM Na-GTP, and 10 mM phosphocreatine-Na_2 (pH 7.2 and 285 mOsM). The MSNs of the DMS were characterized based on their morphology and high resting membrane potential (−70 to −80 mV). Currents with peak amplitudes smaller than 8 pA (depending on the basal noise level of the recording) were excluded from analysis. Changes of more than 20% of access resistance in the neurons were also excluded. Data were acquired and analyzed using pClamp 10.7 software (Molecular Devices).

Image analysis

Acquisition

Digital images were acquired with an Olympus IX71 microscope equipped with a DP72 camera and cellSens software (Olympus) or with an LSM 700 confocal fluorescence microscope system. Confocal images were collected from single optical sections using EC-Plan Neofluar 10×, C-Apochromat 40×, or Plan Apochromat 63× objective lenses.

For quantification of the synaptic density of the bridging collaterals from D1-MSNs in the GPe, the entire GPe was sectioned into 40-μm slices and every fourth slice was taken for quantification. Three or four scan areas (scan area: 100 μm × 100 μm) were acquired from each slice to cover the entire tdTomato or EYFP expression in the GPe.

Analysis

Image analysis was performed using ImageJ v. 1.51g (National Institutes of Health, USA) and Metamorph (Molecular Devices) software. Quantitative analyses for the colocalizations of G2CT expression with the D1-MSN marker, SP, were performed with Metamorph software. Briefly, regions were created around G2CT-positive cells ($G2CT^+$, green), and transferred to the channel showing the SP (red) signal. The SP^+ areas (red) were identified when the fluorescence intensities were stronger than the threshold determined from the local background intensity. The intensity of the overlaid regions (yellow) was quantified, and the data were processed to determine the percentage of colocalization.

To measure the amount of bridging collaterals in G2CT mice, the fluorescence intensity within the GPe was quantified using ImageJ as described previously (Cazorla et al., 2014). The optical density in the whole GPe area and the dorsal striatum area within each slice was measured to obtain the mean fluorescence intensity from each brain area. Every fourth slice from the whole-brain slices that span the GPe was taken. The optical density in the striatum was used as the denominator to normalize the GPe optical density and the normalized data are presented as % striatal optical density.

To directly measure the terminal density of the bridging collaterals, confocal images obtained from the SYP immunofluorescence staining were analyzed with Metamorph software. Briefly, SYP-positive (SYP^+) puncta were identified when 10 or more adjacent pixels above the threshold (average local background intensity) were clustered. If a cluster was more than 50 pixels in length, it was split into smaller puncta. The puncta regions were transferred to the channel that showed the bridging collateral signals (tdTomato- or EYFP-positive), where the $tdTomato^+$ (or $EYFP^+$) areas were also identified in the same fashion. From the overlay, colocalization was determined if more than 50% of the $tdTomato^+$ (or $EYFP^+$) area overlapped with the SYP^+ region.

Florescence-activated cell sorting (FACS) and RT-PCR

Cell dissociation and FACS analyses were performed as previously described (Guez-Barber et al., 2012). The striatal single-cell suspension obtained from the striatal tissue of wild-type or G2CT mice was subjected to FACS to collect G2CT-expressing (GFP^+) neurons. Total RNA was extracted from the sorted cells using the RNeasy Mini Kit (#74104; Qiagen, Germany) and reverse transcribed into cDNA using the amfiRivert cDNA synthesis master mix (#R5600; GenDEPOT, USA). Quantitative gene expression analysis was carried out using the KAPA SYBR FAST Roche LightCycler 480 kit (Kapa Biosystems, USA) and the LC 480 real-time PCR thermocycler (Roche, Switzerland). The primers used in the study were as follows:

D1R_foward, 5'-AGGGAGACTAAAGTCCTG-3';
D1R_reverse, 5'-CCTAAGAGGGTCGAGAAT-3';
D2R_forward, 5'-CTCCCTTAAGACGATGAG-3';
D2R_reverse, 5'-GGTGGTATAGATGATGGG-3';
Glyceraldehyde-3-phosphate dehydrogenase (GAPDH)_forward, 5'-AACTTTGGCATTGTGGAAGG-3';
GAPDH_reverse, 5'-CACATTGGGGGTAGGAACAC-3'

The $2^{-\Delta\Delta Ct}$ method was used to analyze the relative quantifi-

cation of gene expression in each group, and GAPDH expression was used as a reference.

Statistical analyses

All statistical analyses were performed using the IBM SPSS Statistics software (ver. 24; IBM, USA). We used the Student's *t*-test for statistical comparisons of the image analysis data, dendritic spine analysis, and electrophysiological data except for the data sets that did not follow a normal distribution. For data without a normal distribution, the Mann–Whitney test was used as a non-parametric unpaired *t*-test. Wilcoxon signed ranks test for immunoblot assays and two-way ANOVA with *post hoc* Student's *t*-test were used for all behavioral tests, except the DREADD experiments. For the DREADD experiments involving the EPM test, we used two-way repeated ANOVA with *post hoc* Student's *t*-tests (for the drug effect) and paired *t*-tests (for the stress effect) because the same animals were tested in the EPM before and after PRST exposure. The Kolmogorov–Smirnov test (K–S test) was used for comparisons of the cumulative probability distributions. All data are presented as mean ± SEM. $P < 0.05$ was considered statistically significant.

RESULTS

Interfering with AMPAR endocytosis caused alterations in synaptic transmission in the striatum of G2CT transgenic mice

We generated a transgenic mouse line that expresses a peptide derived from the AP2 binding region in the GluA2 recep-

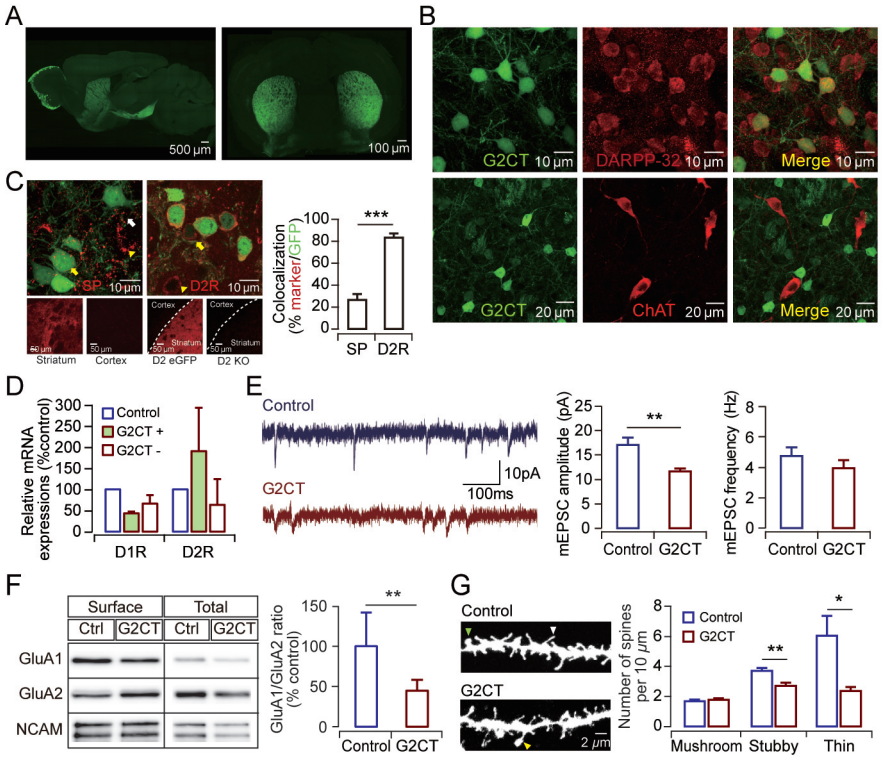

Fig. 1. Synaptic weakening of MSNs in the G2CT transgenic mice is accompanied by biochemical and structural changes at synapses. (A) Expression of the G2CT peptide is shown in the sagittal (left) and coronal (left) sections from G2CT transgenic mouse. (B) Representative images of double immunostaining displaying G2CT-positive cells (green) with DARPP-32 (top, red) or choline acetyltransferase (ChAT; bottom, red). (C) Representative images of double immunostaining displaying G2CT-expressing MSNs (green) with substance P (SP; red, left), or D2R (red, middle) in the dorsal striatum of G2CT mice (yellow arrows, $G2CT^+SP^+$ or $G2CT^+D2R^+$ cells; white arrow, $G2CT^+SP^-$ or $G2CT^+ENK^-$ cells; yellow arrowheads, $G2CT^-SP^+$ or $G2CT^-ENK^+$ cells). Negative control images showing SP immunostaining in the cortex and D2R immunostaining in the striatum of D2R knockout mouse (D2-KO) are shown below with positive staining images for comparison. The quantified results are shown in a graph on the right (SP, n = 8 slices from three G2CT mice; D2R, n = 15 slices from four G2CT mice). (D) Quantitative gene expression analysis from the FACS-sorted MSNs of the G2CT mice. The graph is plotted as the relative expression levels normalized to the expression level in control mice (control, n = 3 mice; G2CT, n = 3 mice). (E) Representative mEPSC traces from the control mice (top) and the G2CT mice (bottom) are shown on the left. Quantified results of the average peak amplitude (middle) and the frequency (right) of the mEPSCs are shown in the graphs (control, n = 8 cells; G2CT, n = 9 cells). (F) Surface biotinylation assays. Representative immunoblot images (left) and quantified results (right) are shown (control, n = 10 mice; G2CT, n = 10 mice). (G) Dendritic spine analysis in the MSNs. Representative images of dendritic spines (left) and the results of quantitative morphological analysis of the dendritic spines of striatal MSNs (right) are shown (control, n = 16 cells; G2CT, n = 18 cells). In all graphs, blue bars represent control mice and red bars represent G2CT mice. $*P < 0.05$, $**P < 0.01$, $***P < 0.001$.

tor (G2CT), which has been shown to prevent AMPAR endocytosis (Lee et al., 2002; Yoon et al., 2009). G2CT is strongly expressed in the striatum and the olfactory bulb but barely expressed elsewhere in these mice (Fig. 1A). Most of the striatal cells that expressed G2CT were MSNs, showing colocalization with the 32-kDa dopamine and cyclic AMP-regulated phosphoprotein (DARPP-32) but not with choline acetyltransferase (Fig. 1B). Although both D1-MSN and D2-MSN expressed G2CT in the transgenic mice, quantitative analyses revealed that there was bias toward expression in D2-MSNs (Figs. 1C and 1D)(U = 8, P = 0.008, Mann–Whitney U test). The basal synaptic transmission was altered in the MSNs of the transgenic mice as analysis of the miniature EPSCs (mEPSCs) for these cells revealed that the peak current amplitudes were significantly smaller (t(15) = 3.384, P = 0.0041, Student's t-test) in the G2CT-expressing MSNs than in the MSNs of the control mice (Fig. 1E). The changes in the basal synaptic transmission were accompanied by molecular and structural modifications at the synapses. The subunit composition of surface-expressed AMPARs (GluA1/GluA2 ratio) (Z = –2.803, P = 0.0051, Wilcoxon signed rank test) and the density of dendritic spines ($Control_{Stubby}$ vs $G2CT_{Stubby}$, t(32) = 3.266, P = 0.0026; $Control_{Thin}$ vs $G2CT_{Thin}$, t(17) = 2.705, P = 0.015, Student's t-test) were significantly lower in the striatum of G2CT mice (Figs. 1F and 1G). A significant difference in the GluA1/GluA2 ratio may indicate a relative difference in the level of GluA2-lacking AMPARs on the surface, which should influence synaptic integration and neuronal excitability (Hume et al., 1991; Liu and Zukin, 2007). Collectively, these data indicate that G2CT expression in the striatal MSNs led to synaptic weakening accompanied by molecular and structural changes, which should have an impact on the basal ganglia network function.

G2CT mice display increased behavioral inhibition after being exposed to PRST

We next examined the behaviors of G2CT mice, which should be under the control of the basal ganglia network. A battery of behavioral tests revealed that the behaviors of the G2CT mice under PRST were different from those of control mice. In the basal state without PRST, the behavior of the G2CT mice did not differ from that of the control mice in the EPM test. However, when the animals were exposed to PRST overnight prior to the test, the G2CT mice demonstrated behavioral alterations. While both the control and the G2CT transgenic mice showed decreased locomotor activity in the open arms ($F(1,44)_{Stress}$ = 10.254, P = 0.003, two-way ANOVA) (Fig. 2A), the duration and speed of the ambulatory behavior in the open arms were significantly decreased in the G2CT transgenic mice after PRST exposure (duration, $F(1,44)_{genotype}$ = 6.796, P = 0.012; speed, $F(1,44)_{Stress}$ = 10.857, P = 0.002, two-way ANOVA) (Figs. 2B and 2C). The G2CT mice also demonstrated a significant decrease in head-dipping behavior after PRST exposure ($F(1,44)_{genotype\ x\ Stress}$ = 4.419, P = 0.041, $F(1,44)_{Stress}$ = 11.118, P = 0.002, two-way ANOVA) (Fig. 2D). A decrease in the active behaviors of the G2CT mice after PRST exposure was also observed in the marble-burying test ($F(1,30)_{genotype}$ = 18.596, P = 0.0002,

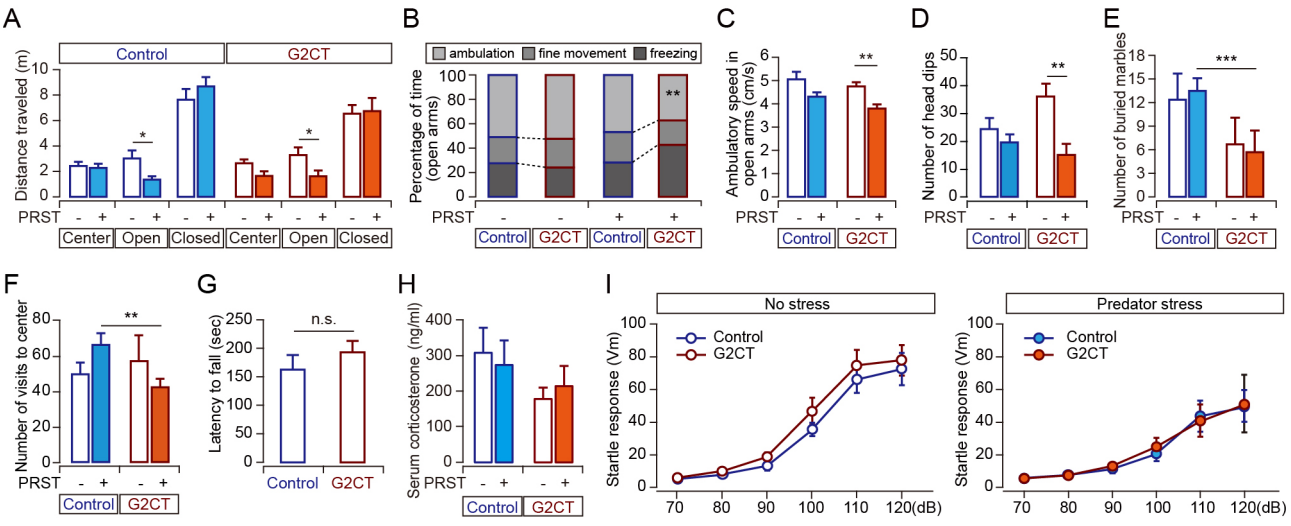

Fig. 2. G2CT mice exhibit altered responses to PRST. (A-D) Behavioral responses in the EPM test with PRST exposure ($Control_{Naïve}$, n = 14, $Control_{PRST}$, n = 14, $G2CT_{Naïve}$, n = 10, $G2CT_{PRST}$, n = 10). Locomotor activity in each arm during the EPM (A), movement analysis in the open arms (B), ambulatory speed in the open arms (C), and the number of head dips (D) are shown. (E) Digging behavior was measured in the marble burying test ($Control_{Naïve}$, n = 8, $Control_{PRST}$, n = 13, $G2CT_{Naïve}$, n = 5, $G2CT_{PRST}$, n = 8). (F) Number of crosses between central and peripheral zones in the OFT ($Control_{Naïve}$, n = 8, $Control_{PRST}$, n = 13, $G2CT_{Naïve}$, n = 6, $G2CT_{PRST}$, n = 10). (G) Latency to fall in the accelerating rotarod test (control, n = 9 mice; G2CT, n = 9 mice). (H) Blood corticosterone levels were measured before and after PRST exposure (control, n = 3 mice, G2CT, n = 7 mice). (I) Acoustic startle responses in naïve state (left) and stressed state (right) ($Control_{naïve}$, n = 7, $Control_{PRST}$, n = 6, $G2CT_{naïve}$, n = 8, $G2CT_{PRST}$, n = 6). In all graphs, blue represents control mice and red represents G2CT mice. Data collected from stress-naïve (PRST-) mice are shown in open bars and data from PRST-exposed (PRST+) mice are shown in filled bars. $*P < 0.05$, $**P < 0.01$, $***P < 0.001$.

two-way ANOVA) and the open field test (OFT) ($F(1,44)_{genotype\ x\ Stress} = 4.196$, $P = 0.049$, two-way ANOVA) (Figs. 2E and 2F), suggesting that overall suppression of active risk-assessment or defensive behaviors occurred in the G2CT mice. However, there were neither general motor deficits nor abnormal hormonal responses to PRST in the G2CT mice (Figs. 2G and 2H). Additionally, there was no difference in the reflexive startle response between the G2CT and control mice, indicating that the decrease in motor responses to PRST is specific to voluntary movement (Fig. 2I).

Collaterals from D1-MSNs within the GPe might control the output balance of basal ganglia circuitry

While the expression of G2CT in the MSNs appears to have caused synaptic weakening, the G2CT mice displayed increased behavioral inhibition under PRST. This led us to postulate that some additional mechanisms other than a simple bias in balance between the activity of the two pathways might underlie the phenotypes of the G2CT mice. Single neuron tracing studies of striatofugal projections have revealed that the majority of striatonigral neurons send a substantial

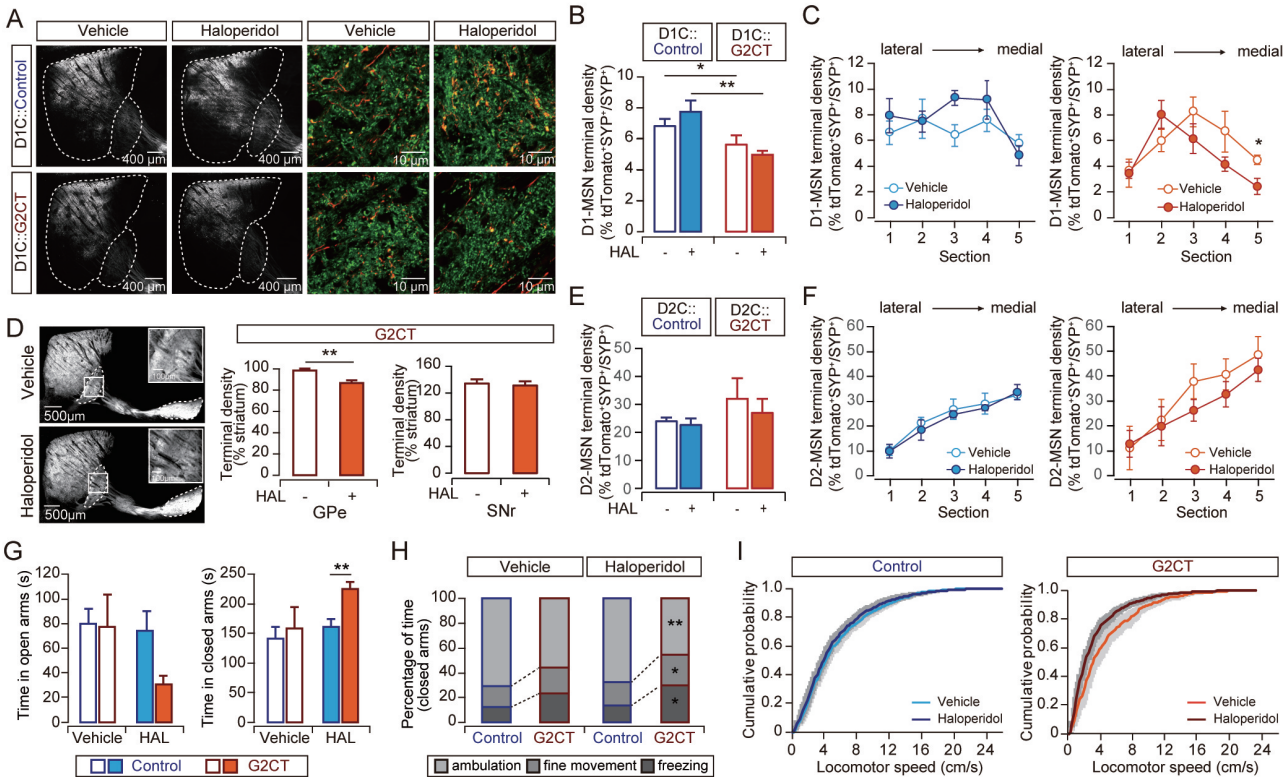

Fig. 3. Amount of bridging collaterals is correlated with stress-related behavior. (A) Representative images of the collateral terminals of D1-MSNs within the GPe. Mice (D1C::Control or D1C::G2CT) were injected with AAV-DIO-tdTomato to visualize D1-MSNs. Sagittal sections showing overall distribution of D1-MSNs and their axons are shown on the left (the striatum and the GPe areas are marked by white dashed lines). Higher magnification images showing the axons of D1-MSNs (red) and synaptophysin (SYP, green) immunostaining are shown on the right. We quantified the overlapping yellow puncta ($tdTomato^+SYP^+$) as the collateral terminals. (B) Quantification of the collateral terminals of the D1-MSNs within the GPe ($D1C::Control_{vehicle}$ n = 3 mice; $D1C::G2CT_{vehicle}$, n = 5 mice; $D1C::Control_{haloperidol}$, n = 4 mice; $D1C::G2CT_{haloperidol}$, n = 4 mice; five sections/mouse). (C) Lateral to medial distribution of the D1-MSN collateral terminal density in the GPe of D1C::Control (left) or D1C::G2CT (right). (D) Representative images of the sagittal sections from G2CT mice (vehicle- or haloperidol-injected) are shown (left). Insets are showing magnified images of the GPe. The results of the quantitative analysis for the fluorescence intensity in the GPe and SNr are shown in a graph (right). Fluorescence intensity of the whole striatum from each section was used for normalization ($G2CT_{Vehicle}$, 24 slices from n = 6 mice; $G2CT_{Haloperidol}$, 32 slices from n = 8 mice). (E) Quantification of the terminals of the D2-MSNs within the GPe of AAV-DIO-tdTomato-injected D2C::Control or D2C::G2CT mice ($D2C::Control_{vehicle}$ n = 5 mice; $D2C::G2CT_{vehicle}$, n = 5 mice; $D2C::Control_{haloperidol}$, n = 7 mice; $D2C::G2CT_{haloperidol}$, n = 5 mice; 5 sections/mouse). (F) Lateral to medial distribution of the D2-MSN terminal density in the GPe of AAV-DIO-tdTomato-injected D2C::Control mice (left) or D2C::G2CT (right). (G-I) Behavioral analysis of haloperidol-injected mice in the EPM test ($Control_{Vehicle}$, n = 9, $Control_{Haloperidol}$, n = 9, $G2CT_{Vehicle}$, n = 6, $G2CT_{Haloperidol}$, n = 8; all groups were exposed to PRST in this experiment). Time spent in the open arms (left) and closed arms (right) (G), movement analysis in the closed arms (H), cumulative probability plot of the locomotor speed in the closed arms (I) are shown. In all graphs, blue represents control mice, and red represents G2CT mice. Data collected from vehicle-injected mice are shown in open bars or circles, and data from haloperidol-injected mice are shown in filled bars or circles. In Fig. 3I, lighter colors indicate vehicle-injected mice and darker colors indicate haloperidol-injected mice. $*P < 0.05$, $**P < 0.01$.

number of axon collaterals to the GPe (Fujiyama et al., 2011). These "bridging collaterals" appear to change dynamically and play a crucial role in fine-tuning the output activity of the basal ganglia network. Interestingly, it has been shown that changes in neuronal excitability of D2-MSNs control the density of the bridging collaterals in the GPe (Cazorla et al., 2014). We therefore investigated the possibility that a change in the amount of bridging collaterals could affect the behavior of the G2CT mice in response to PRST exposure. To examine the amount of bridging collaterals in the G2CT mice, we injected AAV-DIO-tdTomato virus into D1-CRE::G2CT compound transgenic mice for specific labeling of D1-MSNs in the G2CT transgenic mice background. Then, we chronically administered haloperidol, a D2-receptor antagonist that has been shown to effectively reduce the level of bridging collaterals (Cazorla et al., 2014). First, we found that the terminal field density of bridging collaterals was significantly lower in the G2CT mice than in control mice in the basal state. This result implies that the behavioral inhibition we observed in the G2CT mice might indeed have been due to a decrease in the amount of bridging collaterals. Furthermore, 2 weeks of haloperidol treatment (0.5 mg/kg per injection, three injections/day) produced a further decrease in bridging collaterals in the G2CT mice ($F(1,78)_{Genotype} = 16.058$, $P = 0.00014$, two-way ANOVA; $Control_{Vehicle}$ vs $G2CT_{Vehicle}$, $t(37) = 2.216$, $P = 0.033$; $Control_{Haloperidol}$ vs $G2CT_{Haloperidol}$, $t(41) = 3.454$, $P = 0.0013$, *post hoc* Student's *t*-test) (Figs. 3A and 3B). Interestingly, the change in the level of bridging collaterals was particularly apparent in the medial sections of the GPe, which receive major input from the DMS ($F(1,13)_{Section\#5\_Drug} = 5.552$, $P = 0.035$, two-way ANOVA; $G2CT_{Section\#5\_Vehicle}$ vs $G2CT_{Section\#5\_Haloperidol}$, $t(8) = 2.822$, $P = 0.022$, *post hoc* Student's *t*-test) (Fig. 3C). The decrease was also reflected in the overall fluorescence intensity within the GPe ($t(12) = 3.679$, $P = 0.003$, Student's *t*-test), while the terminal density in the SNr was not changed (Fig. 3D). In contrast, the density of the striatopallidal terminals did not change significantly in response to haloperidol treatment (Figs. 3E and 3F). The decrease in the level of bridging collaterals was accompanied by increases in anxiety (time spent in the closed arms, $F(1,29)_{Genotype} = 4.530$, $P = 0.042$, two-way ANOVA) (Fig. 3G) and behavioral inhibition. The ambulation ($F(1,28)_{Genotype} = 12.303$, $P = 0.002$) (Fig. 3H) and locomotor speed in the closed arms ($G2CT_{Vehicle}$ vs $G2CT_{Haloperidol}$, $Z = 2.361$, $P = 3.0e\text{-}05$, two-sample K–S test) (Fig. 3I) were significantly lower in the haloperidol-treated G2CT mice than in those that received vehicle.

If indeed the level of bridging collaterals regulates behavioral responses under stress, we reasoned that an increase in bridging collaterals should reverse the passive coping responses of G2CT mice. It has been shown that modulating the activity of striatal neurons can dynamically control the density of direct pathway collaterals (Cazorla et al., 2014). We, therefore, manipulated the activity of the DMS in the G2CT mice by injecting AAV-hM3Dq and administering CNO daily for 2 weeks (Fig. 4A). This treatment appeared to be sufficient to increase the level of the bridging collaterals. The

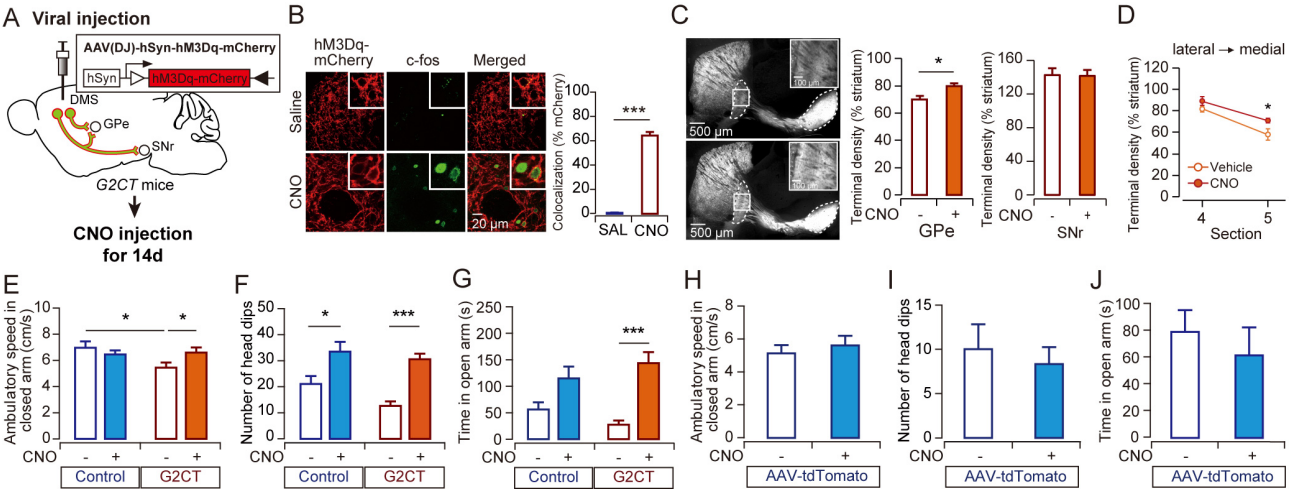

Fig. 4. Increase in bridging collaterals is accompanied by active behaviors. (A) Experimental design. AAV-hM3Dq-mCherry injection into the DMS of control or G2CT mice was followed by 14 days of CNO injection (1 mg/kg, 2 times a day) after recovery. Then the mice were exposed to PRST for 16-18 h prior to being subjected to the EPM test. (B) Representative images of the sagittal sections of vehicle- or CNO-injected G2CT mice. (C and D) The results of the quantitative analysis for the fluorescence intensity in the GPe ($G2CT_{Vehicle}$, n = 7 mice; $G2CT_{CNO}$, n = 7 mice). The fluorescence intensity in the whole GPe and SNr (C) and the lateral-to-medial distribution of the fluorescence intensity in the GPe (D) were measured. The fluorescence intensity of the striatum from each section was used for normalization. (E-G) Behavioral analysis of AAV-hM3D-injected G2CT or control mice in the EPM test ($Control_{Vehicle}$, n = 7; $Control_{CNO}$, n = 8; $G2CT_{Vehicle}$, n = 6; $G2CT_{CNO}$, n = 8). (H-J) Behavioral analysis of AAV-tdTomato-injected wild-type (WT) mice in the EPM test ($WT_{Vehicle}$, n = 4; WT_{CNO}, n = 4; all groups were pre-exposed to PRST in this experiment). Ambulatory speed in the closed arms (E and H), number of head dips (F and I), and time spent in the open arms (G and J) are shown. In all graphs, blue represents control mice and red represents G2CT mice. Data collected from vehicle-treated (CNO-) mice are shown in open bars or circles, and data from CNO-treated (CNO+) mice are shown in filled bars or circles. $*P < 0.05$, $***P < 0.001$.

overall fluorescence in the GPe, but not in the SNr, of the G2CT mice was significantly increased after chronic DMS activation ($t(12) = -2.471$, $P = 0.029$, Student's *t*-test) (Figs. 4B and 4C) and was most prominent in the medial sections (Section#5$_{Vehicle}$ vs Section#5$_{CNO}$, $t(7.926) = -2.319$, $P = 0.049$, Student's *t*-test) (Fig. 4D). In contrast to the decrease in the bridging collaterals, an increase in the bridging collaterals was accompanied by increased active behaviors such as higher ambulatory speed in the closed arms and more frequent head dips (ambulatory speed in the closed arms, $F(1,25)_{Genotype\ x\ Drug} = 5.020$, $P = 0.034$, two-way ANOVA; head dips, $F(1,25)_{Drug} = 25.656$, $P = 0.00031$, two-way ANOVA) (Figs. 4E and 4F). Furthermore, anxiolysis was observed in CNO-treated G2CT mice (time spent in the open arms, $F(1,25)_{Drug} = 21.891$, $P = 0.000086$, two-way ANOVA) (Fig. 4G). However, these behavioral changes were not observed in CNO-treated mice injected with AAV-tdTomato, excluding the possibility that CNO itself might have caused the change due to its metabolization to clozapine (Figs. 4H-4J) (Manvich et al., 2018). These results suggest that dynamic changes in the collaterals from D1-MSNs within the GPe regulate anxiety and stress-related behavior.

DISCUSSION

Distinct roles for the two parallel basal ganglia pathways were proposed in the classical models of the basal ganglia circuit functions (Albin et al., 1989; Graybiel, 2000; Kravitz et al., 2010). These models suggest that the direct pathway promotes movement while the indirect pathway inhibits movement and that these pathways are differentially modulated by dopamine. In addition to their direct motor regulations, these two pathways have also been implicated in adaptive learning (Hikida et al., 2010). The functional diversity of the basal ganglia network might be explained by the parallel organization of basal ganglia-thalamocortical circuits (Alexander et al., 1986). For example, reward-related processing, including drug addiction-associated processing, might be achieved through the limbic loop in which the inputs from the anterior cingulate areas as well as from the limbic system (e.g., amygdala) to the ventral striatum are further processed through the connections to the ventral pallidum and parafascicular/mediodorsal nucleus of the thalamus (Kim et al., 2017b; 2018). In contrast, the associative loop consists of inputs from the dorsolateral prefrontal cortex and lateral orbitofrontal cortex into the caudate nucleus (rodent DMS) and the thalamic subdivisions such as the ventral anterior pars principalis. The caudate nucleus has been implicated in emotional responses (Bhatia and Marsden, 1994; Carretie et al., 2009). Our current study has focused on the functional role of changes in circuitry starting from the DMS in stress-related behaviors since we had previously shown that the viral vector-mediated expression of G2CT in the DMS, but not in the dorsolateral striatum (DLS), altered anxiety-related behavior (Lee et al., 2015). Animal behavior is controlled by either goal-directed or habitual mode of action selection (Dolan and Dayan, 2013). Many studies in rodents and humans have found that the neural basis of behavioral transitions from goal-directed to habitual mode is a shift of neural control from associative (DMS) to sensorimotor (DLS) fronto-striatal circuits (Alexander et al., 1986; Dolan and Dayan, 2013; Yin et al., 2009). Action initiation in goal-directed mode requires careful consideration of probability of achieving a goal in a given investment, which is likely to be gravely influenced

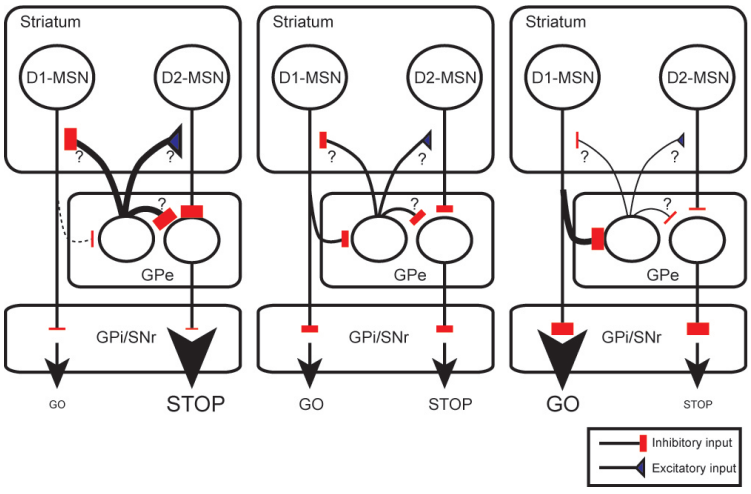

Fig. 5. Proposed model of the regulatory function of the bridging collaterals for behavioral controls in the basal ganglia network. In response to a decrease in the activity of D2-MSNs, the amount of bridging collaterals is decreased (left) from the basal level (center). We hypothesize that the bridging collaterals innervate a distinct neuronal population from prototypic neurons that receive input from D2-MSNs in the GPe. These regulator neurons may be boosting the function of the indirect pathway (possibly by activating D2-MSNs, inhibiting GPe prototypic neurons, or inhibiting D1-MSNs). A decrease in inhibition produced by the bridiging collaterals may therefore result in increased behavioral inhibition. In contrast, an increase in bridging collaterals (right) may lead to greater suppressions on the regulator neurons, which results in increased action initiations. For the simplicity of the diagram, the subthalamic nucleus that receive input from the GPe is omitted.

by the presence of stressors such as predator. Our results demonstrating that circuit dynamics within the medial part of the basal ganglia network is sufficient to control stress-related behaviors conform to this functional distinction between the DMS and the DLS.

The mechanism by which the overall basal ganglia output activity is regulated is currently uncertain. Although recent studies utilizing optogenetic or chemogenetic tools have revealed distinct functional roles for each pathway (Carvalho Poyraz et al., 2016; Ferguson et al., 2011; Hikida et al., 2010; Kravitz et al., 2010; Lobo et al., 2010), how these two pathways are coordinated in natural settings is largely unknown. An *in vivo* imaging study showed that the two pathways are concurrently activated during action initiation, which was further supported by a study demonstrating that both pathways are required for action sequence initiation using state-dependent optogenetic manipulations (Cazorla et al., 2014; Tecuapetla et al., 2016). Therefore, a sophisticated interplay between the two pathways is likely to influence the selection of an action in a given situation. Dynamic reorganization of axon collaterals from the D1-MSNs in the GPe might play an important role in balancing or coordinating crosstalk between the two pathways. Increased neuronal excitability induced by either the overexpression of the D2-receptor or the suppression of inward rectifier potassium channels in D2-MSNs has induced a significant increase in the direct pathway collaterals in the GPe (Cazorla et al., 2012; 2014). A decrease in the level of the bridging collaterals in our G2CT mice is likely to have been caused by altered synaptic transmissions in the striatum. Lower amplitudes for the mEPSCs, fewer dendritic spines, and lower GluA1/GluA2 ratios in the G2CT mice compared those of the control mice are expected to lead to reduced neuronal activation, which might have induced a network reorganization including changes in the amount of bridging collaterals. The reduced level of bridging collaterals in the G2CT mice appears to have induced an increase in passive coping behavior under stress. The G2CT mice displayed a tendency of reduced locomotor activity, though not significant, even without PRST exposure, which might have been caused by low level of stress related to the experimental conditions and apparatuses. An additional decrease in the active behavior of the G2CT mice was observed when the mice were chronically treated with haloperidol, which induced further reduction in the number of bridging collaterals in the GPe. The functional role of the bridging collaterals was also supported by reverse manipulation by which the density of the bridging collaterals was increased, with a concomitant increase in the active coping behavior. While both D1-MSNs and D2-MSNs are inhibitory GABAergic neurons, our data suggest that the bridging collateral inputs and D2-MSNs' inputs to the GPe may exert opposite effects on behavioral control. A decrease in the bridging collaterals induced an increase in passive behavior that is caused by indirect pathway activation, which suggests that the bridiging collaterals might antagonize the function of the indirect pathway activation (Fig. 5). This requires that a distinct circuitry be present for the bridging collateral input in the GPe from that of prototypical neurons receiving input from the D2-MSNs. It is known that there exist different types of neurons in the GPe, such as arkypallidal and prototypic neurons, with distinct molecular markers and connectivity (Abdi et al., 2015). It warrants further studies to examine whether different inputs to the GPe preferentially target separate classes of neurons. It is not clear how neuronal activity of the striatum can lead to dynamic changes in the bridging collaterals. It has been shown that recurrent network activity in the cortico-basal ganglia-thalamo-cortical loop regulates excitatory innervation to the striatum during development (Kozorovitskiy et al., 2012). It is possible that a similar mechanism might be operating in adult basal ganglia network to support flexible behavioral learnings. Collectively, these results indicate that bridging collaterals critically influence behavioral response under stress by controlling the balance of the basal ganglia circuitry.

In conclusion, our findings suggest that the basal ganglia network plays an important role in modulating stress-related behavior. The interconnection between the two pathways at the GPe appears to be crucial for balancing the output activity of the basal ganglia. Genetic predispositions or environmental effects on stress responses might be manifested, at least in part, through changes in bridging collaterals. Our study provides a new opportunity to understand the control mechanisms for stress-coping behavior and to identify targets for therapeutic intervention in stress-related disorders.

Disclosure

The authors have no potential conflicts of interest to disclose.

ACKNOWLEDGMENTS

This study was supported by the Basic Science Research Program through the National Research Foundation of Korea (NRF) funded by the Ministry of Science, ICT, & Future Planning of the Republic of Korea (NRF-2017R1A2B4007288) and a Korea University research grant to BJY and in part by the KIST Institutional Program (project No. 2E26640) to HYK. We thank Sooji Kim and Sangheon Ji for technical assistance.

ORCID

Young Lee https://orcid.org/0000-0002-5363-0917
Na-Eun Han https://orcid.org/0000-0003-3503-3913
Wonju Kim https://orcid.org/0000-0002-0000-8470
Jae Gon Kim https://orcid.org/0000-0002-5562-1563
In Bum Lee https://orcid.org/0000-0002-9695-7485
Su Jeong Choi https://orcid.org/0000-0001-5479-8167
Heejung Chun https://orcid.org/0000-0002-6451-1542
Misun Seo https://orcid.org/0000-0003-2887-3594
C. Justin Lee https://orcid.org/0000-0002-3555-0980
Hae-Young Koh https://orcid.org/0000-0002-5991-0530
Joung-Hun Kim https://orcid.org/0000-0001-6716-2037
Ja-Hyun Baik https://orcid.org/0000-0002-4607-924X
Mark F. Bear https://orcid.org/0000-0002-9903-2541
Se-Young Choi https://orcid.org/0000-0001-7534-5167
Bong-June Yoon https://orcid.org/0000-0002-8372-1000

REFERENCES

Abdi, A., Mallet, N., Mohamed, F.Y., Sharott, A., Dodson, P.D., Nakamura, K.C., Suri, S., Avery, S.V., Larvin, J.T., Garas, F.N., et al. (2015). Prototypic and arkypallidal neurons in the dopamine-intact external globus pallidus. J. Neurosci. *35*, 6667-6688.

Albin, R.L., Young, A.B., and Penney, J.B. (1989). The functional anatomy of basal ganglia disorders. Trends Neurosci. *12*, 366-375.

Alexander, G.E., DeLong, M.R., and Strick, P.L. (1986). Parallel organization of functionally segregated circuits linking basal ganglia and cortex. Annu. Rev. Neurosci. *9*, 357-381.

Bateup, H.S., Santini, E., Shen, W., Birnbaum, S., Valjent, E., Surmeier, D.J., Fisone, G., Nestler, E.J., and Greengard, P. (2010). Distinct subclasses of medium spiny neurons differentially regulate striatal motor behaviors. Proc. Natl. Acad. Sci. U. S. A. *107*, 14845-14850.

Bhatia, K.P. and Marsden, C.D. (1994). The behavioural and motor consequences of focal lesions of the basal ganglia in man. Brain *117*, 859-876.

Carretie, L., Rios, M., de la Gandara, B.S., Tapia, M., Albert, J., Lopez-Martin, S., and Alvarez-Linera, J. (2009). The striatum beyond reward: caudate responds intensely to unpleasant pictures. Neuroscience *164*, 1615-1622.

Carvalho Poyraz, F., Holzner, E., Bailey, M.R., Meszaros, J., Kenney, L., Kheirbek, M.A., Balsam, P.D., and Kellendonk, C. (2016). Decreasing striatopallidal pathway function enhances motivation by energizing the initiation of goal-directed action. J. Neurosci. *36*, 5988-6001.

Cazorla, M., de Carvalho, F.D., Chohan, M.O., Shegda, M., Chuhma, N., Rayport, S., Ahmari, S.E., Moore, H., and Kellendonk, C. (2014). Dopamine D2 receptors regulate the anatomical and functional balance of basal ganglia circuitry. Neuron *81*, 153-164.

Cazorla, M., Shegda, M., Ramesh, B., Harrison, N.L., and Kellendonk, C. (2012). Striatal D2 receptors regulate dendritic morphology of medium spiny neurons via Kir2 channels. J. Neurosci. *32*, 2398-2409.

Choi, T.Y., Lee, S.H., Kim, Y.J., Bae, J.R., Lee, K.M., Jo, Y., Kim, S.J., Lee, A.R., Choi, S., Choi, L.M., et al. (2018). Cereblon maintains synaptic and cognitive function by regulating BK channel. J. Neurosci. *38*, 3571-3583.

Cui, G.H., Jun, S.B., Jin, X., Pham, M.D., Vogel, S.S., Lovinger, D.M., and Costa, R.M. (2013). Concurrent activation of striatal direct and indirect pathways during action initiation. Nature *494*, 238-242.

Deacon, R.M. (2006). Digging and marble burying in mice: simple methods for in vivo identification of biological impacts. Nat. Protoc. *1*, 122-124.

DeLong, M.R. (1990). Primate models of movement disorders of basal ganglia origin. Trends Neurosci. *13*, 281-285.

Dolan, R.J. and Dayan, P. (2013). Goals and habits in the brain. Neuron *80*, 312-325.

Ferguson, S.M., Eskenazi, D., Ishikawa, M., Wanat, M.J., Phillips, P.E., Dong, Y., Roth, B.L., and Neumaier, J.F. (2011). Transient neuronal inhibition reveals opposing roles of indirect and direct pathways in sensitization. Nat. Neurosci. *14*, 22-24.

Fujiyama, F., Sohn, J., Nakano, T., Furuta, T., Nakamura, K.C., Matsuda, W., and Kaneko, T. (2011). Exclusive and common targets of neostriatofugal projections of rat striosome neurons: a single neuron-tracing study using a viral vector. Eur. J. Neurosci. *33*, 668-677.

Gerfen, C.R., Engber, T.M., Mahan, L.C., Susel, Z., Chase, T.N., Monsma, F.J., Jr., and Sibley, D.R. (1990). D1 and D2 dopamine receptor-regulated gene expression of striatonigral and striatopallidal neurons. Science *250*, 1429-1432.

Graybiel, A.M. (2000). The basal ganglia. Curr. Biol. *10*, R509-R511.

Guez-Barber, D., Fanous, S., Harvey, B.K., Zhang, Y., Lehrmann, E., Becker, K.G., Picciotto, M.R., and Hope, B.T. (2012). FACS purification of immunolabeled cell types from adult rat brain. J. Neurosci. Methods *203*, 10-18.

Hikida, T., Kimura, K., Wada, N., Funabiki, K., and Nakanishi, S. (2010). Distinct roles of synaptic transmission in direct and indirect striatal pathways to reward and aversive behavior. Neuron *66*, 896-907.

Hume, R.I., Dingledine, R., and Heinemann, S.F. (1991). Identification of a site in glutamate receptor subunits that controls calcium permeability. Science *253*, 1028-1031.

Jin, X., Tecuapetla, F., and Costa, R.M. (2014). Basal ganglia subcircuits distinctively encode the parsing and concatenation of action sequences. Nat. Neurosci. *17*, 423-430.

Kawaguchi, Y., Wilson, C.J., and Emson, P.C. (1990). Projection subtypes of rat neostriatal matrix cells revealed by intracellular injection of biocytin. J. Neurosci. *10*, 3421-3438.

Kim, H.F., Amita, H., and Hikosaka, O. (2017a). Indirect pathway of caudal basal ganglia for rejection of valueless visual objects. Neuron *94*, 920-930. e3.

Kim, H.J., Lee, J.H., Yun, K., and Kim, J.H. (2017b). Alterations in striatal circuits underlying addiction-like behaviors. Mol. Cells *40*, 379-385.

Kim, J., Lee, S., Kang, S., Jeon, T.I., Kang, M.J., Lee, T.H., Kim, Y.S., Kim, K.S., Im, H.I., and Moon, C. (2018). Regulator of G-protein signaling 4 (RGS4) controls morphine reward by glutamate receptor activation in the nucleus accumbens of mouse brain. Mol. Cells *41*, 454-464.

Kim, W., Im, M.J., Park, C.H., Lee, C.J., Choi, S., and Yoon, B.J. (2013). Remodeling of the dendritic structure of the striatal medium spiny neurons accompanies behavioral recovery in a mouse model of Parkinson's disease. Neurosci. Lett. *557* Pt B, 95-100.

Kozorovitskiy, Y., Saunders, A., Johnson, C.A., Lowell, B.B., and Sabatini, B.L. (2012). Recurrent network activity drives striatal synaptogenesis. Nature *485*, 646-650.

Kravitz, A.V., Freeze, B.S., Parker, P.R.L., Kay, K., Thwin, M.T., Deisseroth, K., and Kreitzer, A.C. (2010). Regulation of parkinsonian motor behaviours by optogenetic control of basal ganglia circuitry. Nature *466*, 622-626.

Kravitz, A.V., Tye, L.D., and Kreitzer, A.C. (2012). Distinct roles for direct and indirect pathway striatal neurons in reinforcement. Nat. Neurosci. *15*, 816-818.

Kreitzer, A.C. and Malenka, R.C. (2007). Endocannabinoid-mediated rescue of striatal LTD and motor deficits in Parkinson's disease models. Nature *445*, 643-647.

Lambeth, C.R., White, L.J., Johnston, R.E., and de Silva, A.M. (2005). Flow cytometry-based assay for titrating dengue virus. J. Clin. Microbiol. *43*, 3267-3272.

LeDoux, J. (2012). Rethinking the emotional brain. Neuron *73*, 653-676.

Lee, S.H., Liu, L.D., Wang, Y.T., and Sheng, M. (2002). Clathrin adaptor AP2 and NSF interact with overlapping sites of GluR2 and play distinct roles in AMPA receptor trafficking and hippocampal LTD. Neuron *36*, 661-674.

Lee, Y., Lee, H., Kim, H.W., and Yoon, B.J. (2015). Altered trafficking of alpha-amino-3-hydroxy-5-methyl-4-isoxazolepropionic acid-type glutamate receptors (AMPARs) in the striatum leads to behavioral changes in emotional responses. Neurosci. Lett. *584*, 103-108.

Liu, S.J. and Zukin, R.S. (2007). Ca2+-permeable AMPA receptors in synaptic plasticity and neuronal death. Trends Neurosci. *30*, 126-134.

Lobo, M.K., Covington, H.E., 3rd., Chaudhury, D., Friedman, A.K., Sun, H., Damez-Werno, D., Dietz, D.M., Zaman, S., Koo, J.W., Kennedy, P.J., et al. (2010). Cell type-specific loss of BDNF signaling mimics optogenetic control of cocaine reward. Science *330*, 385-390.

Manvich, D.F., Webster, K.A., Foster, S.L., Farrell, M.S., Ritchie, J.C., Porter, J.H., and Weinshenker, D. (2018). The DREADD agonist clozapine N-oxide (CNO) is reverse-metabolized to clozapine and produces clozapine-like interoceptive stimulus effects in rats and mice. Sci. Rep. *8*, 3840.

Mink, J.W. (1996). The basal ganglia: focused selection and inhibition of competing motor programs. Prog. Neurobiol. *50*, 381-425.

Rodriguez, A., Ehlenberger, D.B., Dickstein, D.L., Hof, P.R., and Wearne, S.L. (2008). Automated three-dimensional detection and shape classification of dendritic spines from fluorescence microscopy images. PLoS One *3*, e1997.

Roseberry, T.K., Lee, A.M., Lalive, A.L., Wilbrecht, L., Bonci, A., and Kreitzer,

A.C. (2016). Cell-type-specific control of brainstem locomotor circuits by basal ganglia. Cell *164*, 526-537.

Shen, W.X., Flajolet, M., Greengard, P., and Surmeier, D.J. (2008). Dichotomous dopaminergic control of striatal synaptic plasticity. Science *321*, 848-851.

Stroobants, S., Gantois, I., Pooters, T., and D'Hooge, R. (2013). Increased gait variability in mice with small cerebellar cortex lesions and normal rotarod performance. Behav. Brain Res. *241*, 32-37.

Taverna, S., Ilijic, E., and Surmeier, D.J. (2008). Recurrent collateral connections of striatal medium spiny neurons are disrupted in models of Parkinson's disease. J. Neurosci. *28*, 5504-5512.

Tecuapetla, F., Jin, X., Lima, S.Q., and Costa, R.M. (2016). Complementary contributions of striatal projection pathways to action initiation and execution. Cell *166*, 703-715.

Tecuapetla, F., Koos, T., Tepper, J.M., Kabbani, N., and Yeckel, M.F. (2009). Differential dopaminergic modulation of neostriatal synaptic connections of striatopallidal axon collaterals. J. Neurosci. *29*, 8977-8990.

Tecuapetla, F., Matias, S., Dugue, G.P., Mainen, Z.F., and Costa, R.M. (2014). Balanced activity in basal ganglia projection pathways is critical for contraversive movements. Nat. Commun. *5*, 4315.

Wu, Y., Richard, S., and Parent, A. (2000). The organization of the striatal output system: a single-cell juxtacellular labeling study in the rat. Neurosci. Res. *38*, 49-62.

Yin, H.H., Mulcare, S.P., Hilario, M.R.F., Clouse, E., Holloway, T., Davis, M.I., Hansson, A.C., Lovinger, D.M., and Costa, R.M. (2009). Dynamic reorganization of striatal circuits during the acquisition and consolidation of a skill. Nat. Neurosci. *12*, 333-341.

Yoon, B.J., Smith, G.B., Heynen, A.J., Neve, R.L., and Bear, M.F. (2009). Essential role for a long-term depression mechanism in ocular dominance plasticity. Proc. Natl. Acad. Sci. U. S. A. *106*, 9860-9865.